Large-scale chromatin structure of inducible genes: transcription on a condensed, linear template

Yan Hu, Igor Kireev, Matt Plutz, Nazanin Ashourian, and Andrew S. Belmont

Department of Cell and Developmental Biology, University of Illinois, Urbana, IL 61801

The structure of interphase chromosomes, and in particular the changes in large-scale chromatin structure accompanying transcriptional activation, remain poorly characterized. Here we use light microscopy and in vivo immunogold labeling to directly visualize the interphase chromosome conformation of 1–2 Mbp chromatin domains formed by multi-copy BAC transgenes containing 130–220 kb of genomic DNA surrounding the DHFR, Hsp70, or MT gene loci. We demonstrate near-endogenous transcription levels in the context of large-scale chromatin fibers compacted nonuniformly well above the 30-nm chromatin fiber. An approximately 1.5–3-fold extension of these large-scale chromatin fibers accompanies transcriptional induction and active genes remain mobile. Heat shock–induced Hsp70 transgenes associate with the exterior of nuclear speckles, with Hsp70 transcripts accumulating within the speckle. Live-cell imaging reveals distinct dynamic events, with Hsp70 transgenes associating with adjacent speckles, nucleating new speckles, or moving to preexisting speckles. Our results call for re-examination of classical models of interphase chromosome organization.

Introduction

Our current understanding of how 10- and 30-nm chromatin fibers fold within interphase and mitotic chromosomes, a level of chromatin organization referred to as large-scale chromatin structure, is quite poor. Traditional models typically have pictured interphase chromosomes as formed by a series of looped domains, each consisting of 20–100-kbp DNA regions folded as extended 30-nm chromatin fibers, anchored to a nonhistone chromosome scaffold through SAR/MAR and/or boundary element sequences. In these models, the transition from a transcriptionally inactive to active gene is accompanied by an approximately sixfold decondensation of the looped domain from a 30-nm to 10-nm chromatin fiber.

This traditional model is derived from converging cytological and biochemical experimental directions. The band/interband pattern of insect polytene chromosomes suggested defined chromatin domains with differential chromatin compaction. Polytene chromosome "puffing" during gene activation, and the visualization of RNP covered loops of active loci in lampbrush chromosomes (Callan, 1982), suggested the extensive decondensation of these domains into decondensed chromatin fibers during transcription, as confirmed by ultrastructural analysis (Ericsson et al., 1989). Parallel biochemical experiments demonstrated increased nuclease sensitivity over large regions flanking active gene loci (Igo-Kemenes et al., 1982; Elgin, 1990). More recently, domains of increased nuclease sensitivity were correlated with domains or subdomains of histone acetylation and H3 lysine 4 methylation for the chicken (Litt et al., 2001) and mouse (Bulger et al., 2003) β-globin loci, respectively; these changes can precede actual induction of transcription (Forrester et al., 1986).

Cytology of diploid interphase nuclei, in contrast, has suggested a much higher level of chromatin compaction, even for most active genes. Interphase chromosomes have been variably described as consisting of giant loops of 30-nm chromatin fibers (Yokota et al., 1995), a string of 200–400-nm diameter, ∼1-Mbp foci formed by rosettes of 30-nm chromatin loops

Correspondence to Andrew S. Belmont: asbel@illinois.edu

I. Kireev's present address is Department of Electron Microscopy, A.N. Belozersky Institute of Physico-Chemical Biology, Moscow State University, Moscow, 119899, Russia.

N. Ashourian's present address is Laboratory of Biochemistry and Molecular Biology, National Cancer Institute, Bethesda, MD 20814.

Abbreviations used in this paper: AAD, acidic activation domain; BAC, bacterial artificial chromosome; DHFR, dihydrofolate reductase; DRB, 5,6-dichloro-1-β-D-ribobenzimidazole; Hsp 70, heat shock protein 70; IGC, interchromatin granule clusters; Mbp, megabase pair; mRFP, monomeric red fluorescent protein; MT, metallothionein; qPCR, quantitative PCR; qRT-PCR, quantitative RT-PCR.

The Rockefeller University Press $30.00
J. Cell Biol. Vol. 185 No. 1 87–100
www.jcb.org/cgi/doi/10.1083/jcb.200809196

(Munkel et al., 1999), or folding of 10- and 30-nm chromatin fibers into larger diameter "chromonema" fibers (Belmont and Bruce, 1994; Kireeva et al., 2004; Kireev et al., 2008). Mapping of specific genes by FISH confirms interphase chromosome compaction well beyond that predicted for 30-nm chromatin fibers in mammalian cells (Lawrence et al., 1990), with single, diffraction-limited spots observed for 100–200-kb genomic regions for nearly all gene loci examined (Yokota et al., 1995). Additional FISH experiments show certain gene loci, activated or poised for transcription, protruding from chromosome territories in loops several Mbp in length (Volpi et al., 2000; Mahy et al., 2002; Ragoczy et al., 2003) and with ∼500-fold compaction (Mahy et al., 2002), more than 10-fold greater than expected for extended 30-nm fibers. Analysis of two different 400-kbp chromosome regions by FISH also revealed large-scale chromatin compaction several fold higher than that expected for 30-nm chromatin fibers even after decondensation after gene activation (Muller et al., 2004). Here the problems, however, are the questionable structural preservation associated with FISH procedures, the low resolution provided by light microscopy, and the uncertain location of transcribed sequences relative to the intergenic flanking regions. Classical electron microscopy (EM) methods instead suggest general sites of transcription are enriched at the periphery of regions of highly condensed chromatin regions, with nascent transcripts assumed to correlate with the appearance of "perichromatin fibrils" (Cmarko et al., 1999). In these studies actual visualization of chromatin is challenging due to the EDTA regressive staining method so that structural details of these chromatin masses are limited.

Our long-standing goal has been to develop methods for imaging the large-scale chromatin structure of specific genes, before and after transcriptional activation. As a "first generation" approach, we targeted the VP16 transcriptional acidic activator via lac operator repeats to a large heterochromatin region and observed its unfolding into extended, transcriptionally active large-scale chromatin fibers with an ∼1,000:1 compaction ratio, very different in appearance from that predicted by loop domain models (Tumbar et al., 1999). Similar large-scale chromatin decondensation was observed by light microscopy in second generation approaches, using multi-copy plasmid insertions containing inducible promoters. This was first demonstrated using a large transgene array containing the inducible MMTV promoter (Muller et al., 2001) and later with β-globin regulatory sequences driving a reporter gene construct (Dietzel et al., 2004).

Both these first and second generation approaches are quite artificial, involving short promoter regions embedded in high-copy plasmid transgene arrays, subject to heterochromatin formation associated with transgene silencing.

Here we describe our third generation approach, which examines lac operator tagged, BAC transgenes containing specific mouse or human genes surrounded by large genomic flanking regions and expressed at levels within several fold of the endogenous genes. By analyzing cell clones containing multiple, tandem copies of the BAC transgenes, we were able to create homogeneous, ∼1–2-Mbp chromatin transcriptional domains comprised largely of eukaryotic sequence and including many distal regulatory sequences. Using lac operator/GFP repressor tagging we were able to directly observe the large-scale chromatin conformation and dynamics of these gene regions in live-cells, correlate RNA FISH signals with BAC transgene conformation without the structural perturbations associated with DNA FISH, and visualize transgene ultrastructure using a novel in vivo immunogold labeling procedure minimizing structural perturbation of chromatin structure. These studies provide our closest look to date at the native large-scale chromatin conformation and dynamics of specific gene loci in diploid nuclei before and after 5–200-fold levels of transcriptional induction. We also describe association of the Hsp70 transgenes with nuclear speckles, nuclear bodies enriched in numerous RNA metabolic components, demonstrating accumulation of Hsp70 mRNA within these bodies.

Results

Generation of cell lines containing multiple copies of DHFR, MT, and Hsp70 BAC transgenes

We chose three housekeeping genes, mouse DHFR (dihydrofolate reductase), human MT (metallothionein), and human Hsp70 (heat shock protein 70), whose expression can be induced in most cell lines using well-defined experimental conditions. Four BACs with genomic insert sizes of 114 kb (DHFR, 560M7), 168 kb (DHFR, 057L22), 164 kb (MT), and 171.5 kb (Hsp70) were selected from the CITB Mouse and RPCI-11 Human BAC libraries. Although these four BACs all contain inducible genes, they vary in the number and distribution of inducible and constitutive genes contained within the BAC as well as the sizes of the transcribed genes (Fig. 1).

We used Tn5 transposition to randomly insert a 10-kb, 256mer lac operator direct repeat into the BACs. For the DHFR BACs, a transposable element was created by flanking the lac operator repeats and a prokaryotic selectable marker with two 19-bp Tn5 transposase recognition sequences (Fig. 1 A). The DHFR gene itself served as the eukaryotic selectable marker when transfected into DHFR minus DG44 CHO cells. This bacterial selectable marker was replaced by a kan/neo prokaryotic/eukaryotic selectable marker for the Hsp70 and MT BACs. Transposition was performed on BAC DNA in vitro using purified Tn5 transposase followed by transformation of DNA into *E. coli*, selection of individual colonies, and identification of the transposable element insertion site using DNA sequencing. Maps of the four BACs selected for further analysis show locations of the transposable element insertion sites relative to the expressed genes (Fig. 1 B).

Each BAC was transfected into a DG44 CHO subclone stably expressing an EGFP–dimer lac repressor-NLS (nuclear localization signal) fusion protein (EGFP-lac repressor) and stable clones were selected and screened by GFP fluorescence. A significant number of clones contained a single, diffraction-limited GFP spot of similar, low intensity. These were assumed to represent single copy insertions. However, to provide a sensitive light microscopy assay of changes in large-scale chromatin conformation, we instead focused on cell clones containing

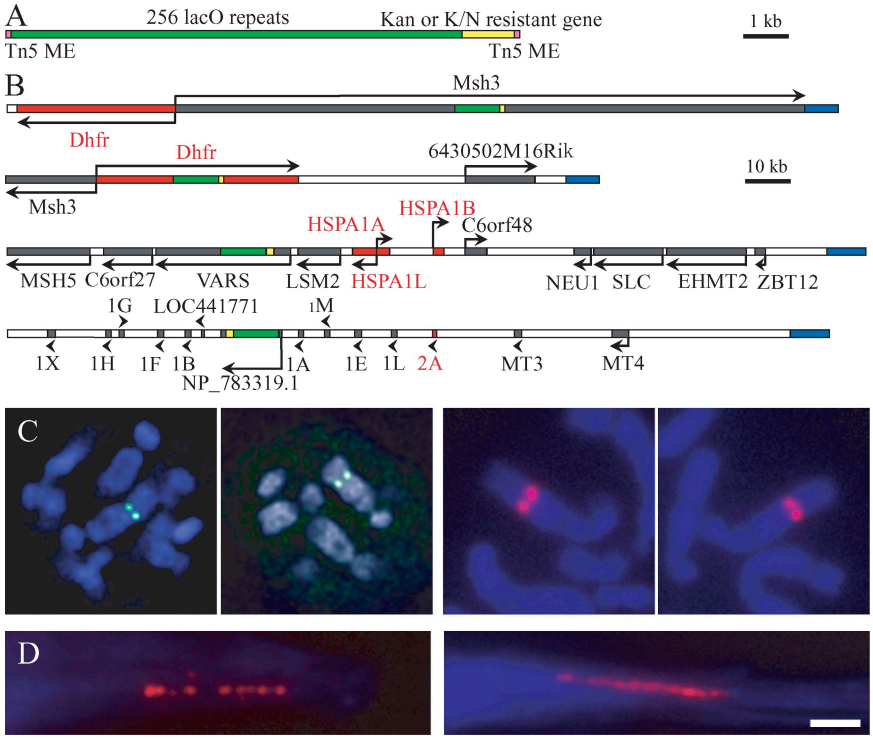

Figure 1. **Generation of stable cell lines with multi-copy, inducible BAC transgenes.** (A) Transposable element with 19-bp Tn5 mosaic ends (red) used to insert 256mer lac operator repeat (green) and selectable marker (yellow) into BACs. (B) BACs used in this study (top to bottom): DHFR 057L22-K-8.32-C-29, DHFR 560M7-K-8.32-C-5, Hsp70 92G8-K/N-8.32-C-2, and Metallothionein 134B2-K/N-8.32-C-8. Inducible genes whose expression we monitored (red), other genes (gray), transposable element (green), and vector backbone (blue) are shown in linear form. (C and D) DNA counterstaining is with DAPI (blue). (C) Transgenes localized in mitotic spreads of the DHFR D10 cell line. Left two panels: lac repressor staining (green); right two panels: FISH (BAC probe, red). (D) Fiber FISH (red) provides copy number estimates with lac operator probe (left) and shows contiguous, tandem BAC insertions with BAC probe (right) for the Hsp70_5 cell line. Bar (C and D), 2 μm.

multiple GFP spots corresponding to multi-copy BAC insertions. Despite the clonal origin of these cells, a variable spot number per nucleus was observed. For three of these BACs, the larger DHFR and the Hsp70 and MT BACs, we selected a cell clone in which a fraction of nuclei showed a similar, maximum number of ~10 GFP spots per nucleus. Most of our experiments concentrated on these three cell clones.

For each clone, intact, metaphase plates or mitotic chromosome spreads showed a fixed chromosomal BAC insertion site and roughly constant BAC insert size (Fig. 1 C; Fig. S1, A and B), suggesting variable large-scale chromatin conformation within a stable, clonal cell population. BAC copy numbers in these clones were estimated first using qPCR. Alternatively, chromatin fiber FISH provided an independent, and likely more accurate measure of mean copy number while also establishing that the multiple copy BACs were present as continuous tandem arrays with no detectable CHO genomic DNA between individual BAC copies (Fig. 1 D; Fig. S1, C and D). BAC copy numbers estimated by qPCR were quite similar and close to the maximum number of roughly 10 GFP spots per nucleus for all three cell lines; similar numbers were obtained for the Hsp70 and DHFR cell lines using chromatin fiber FISH, with the MT clone showing a slightly increased number of BAC copies (17 vs. 9) using chromatin fiber FISH (Table I).

Transcriptional induction of BAC transgenes

A major motivation for moving to this third generation, BAC transgene approach was to analyze changes in large-scale chromatin structure associated with transcriptional activation in a system that more closely approximated the activation of native genes at their normal chromosomal locations. Multi-copy plasmid based

Table I. **BAC copy number estimation and average chromatin compaction ratios**

	DHFR D10_2	Hsp70_5	MT1_1_4
[a]Copy number by real-time PCR	13 (10–16)	10 (8–14)	9 (7–11)
[b]Copy number by Fiber-FISH	11–12	9–10	16–18
BAC size (kb)	187.1	192.6	185.2
Average contour length w/o induction (μm)	0.65	0.52	0.69
[c]Compaction ratio w/o induction	1125:1	1200:1	1550:1
Average contour length w/induction (μm)	1.41	1.51	0.98
[c]Compaction ratio w/induction	520:1	410:1	1090:1

[a]Mean values obtained from more than three individual experiments. Data ranges are in parentheses. Table S1 lists PCR primers used.

[b]Values obtained by counting the numbers of lac operator FISH signals in at least three nuclei which show the best stretched chromatin fibers.

[c]Compaction ratios were calculated using copy numbers based on the mean values of the Fiber-FISH data.

Table II. **Gene expression measured by qRT-PCR**

	Hsp70_5			
	CTRL		HS	
	Endogenous	Transgene	Endogenous	Transgene
[a]Relative	1	0.63 ± 0.11	140 ± 23	200 ± 56
[b]Normalized	1	0.14 ± 0.02	140 ± 23	45 ± 12

	MT1_1_4			DHFR D10
	CTRL	Zn	Log phase	G1 block
		2 h 16 h	(CTRL)	
[c]Relative	1	3.9 ± 0.14 51 ± 8.3	1	0.31 ± 0.046

[a]Expression levels relative to endogenous HSPA1A expression level at control temperature—human specific primers were used for BAC transgene, a 100% rat/mouse conserved sequence (specific for the CHO endogenous HSPA1A copy) was used for the endogenous gene.

[b]Expression levels normalized for copy number estimated by mean of qPCR data (Table I).

[c]Expression levels relative to control.

qRT-PCR was performed on four independent experiments for the Hsp70_5 cell line and three independent experiments for the DHFR D10 and MT1_1_4 cell lines. The comparative $2^{-\Delta\Delta Ct}$ method was used for relative expression level measurements. The β-actin gene was used as the endogenous control to normalize RNA loading. Numbers shown are the mean ± SE. PCR primers are listed in Table S2.

transgenes are subject both to strong position effects and to transgene silencing effects which increase with gene copy number.

We used the Hsp70 BAC multi-copy insertion cell line to carefully compare the level of expression and transcriptional induction of the endogenous gene versus the BAC transgene. To induce Hsp70 expression, we incubated cells at 42ºC for 30 min. Transcript levels were measured by qRT-PCR using species-specific primers before and after heat shock. Hsp70 transcription increased ∼140-fold for the endogenous genes versus ∼200-fold for the transgenes. Normalized by gene copy number, Hsp70 transgene transcript levels were 6–7-fold lower than endogenous Hsp70 transcript levels before heat shock and 3–4-fold lower after heat shock (Table II). Thus, Hsp70 BAC transgene transcription levels were within several fold of the endogenous Hsp70 genes and very similar to the endogenous genes in overall fold induction after heat shock.

DHFR expression varied similarly to literature values reported for chromosomal DHFR amplified genes. CHO DG44 cells are clonally derived CHO cells containing x-ray induced deletions of both endogenous DHFR genes (Urlaub et al., 1986), precluding the comparison of DHFR transgene versus endogenous DHFR transcript levels in the same cells. DHFR expression is present throughout the cell cycle of cycling cells (Feder et al., 1989) but decreases after cell cycle arrest. We blocked cells in a G1 arrest using either serum starvation (Chang et al., 2001) or DMSO treatment (Fiore et al., 2002). In both cases G1 arrest was verified by flow cytometry (unpublished data). G1 arrest led to a 3–4-fold decrease in BAC DHFR transcripts levels, as measured by qRT-PCR (Table II), as compared with a reported ∼10-fold reduction in DHFR transcripts in serum starved versus serum stimulated cells (Ljungman and Hanawalt, 1995; Iwanaga et al., 2004). For the MT gene cluster, we observed 4–50-fold increases in MT2A transgene expression with 2–16 h Zn induction, respectively (Table II). This increase is comparable to reported increases for the endogenous MT2A gene in human prostate epithelial cells and in CHO cells after gene amplification (Albrecht et al., 2008; Singh et al., 2008). Differences in primer efficiency prevented an accurate normalization to endogenous gene expression levels.

An overall large-scale chromatin decondensation accompanies transcriptional induction, but active gene loci remain highly condensed

We directly compared changes in large-scale chromatin structure before and after transcriptional induction for each of the three BAC transgene cell lines. Induction conditions suitable for one transgene served as additional negative controls for the cell lines carrying the other two BAC transgenes.

Interestingly, all three cell lines showed similar levels of large-scale chromatin condensation for the three different BAC transgene arrays, both in the uninduced and induced states (Fig. 2, Table I). Using light microscopy, we measured changes in the number of GFP visible dots as well as changes in the contour length over a curvilinear path linking all of these GFP spots.

In the uninduced state, all three cell lines showed an average of 2.5–3 GFP dots per nucleus (maximum 6) with an average contour length of ∼0.5–0.75 µm (maximum 1.5 µm). After induction, the average number of GFP spots increases to 4–4.5 (maximum 10) and the average contour length increased 1.4–2.9-fold to ∼1.0–1.5 µm (maximum 3.5 µm) (Table I, Fig. S2). Relative to the linear DNA compaction ratio of 30-nm chromatin fibers, the mean compaction ratio for uninduced BAC transgenes was ∼25–50 fold higher (Table I). An ∼1.5–3 fold average decondensation accompanied gene induction, with the minimum observed compaction (175) still several fold higher than 30-nm chromatin fibers. Uninduced and induced chromatin compaction ratios were similar for the three different transgenes even though transcription levels varied significantly (Table II). The above data does not exclude the possibility that the transcribed genes

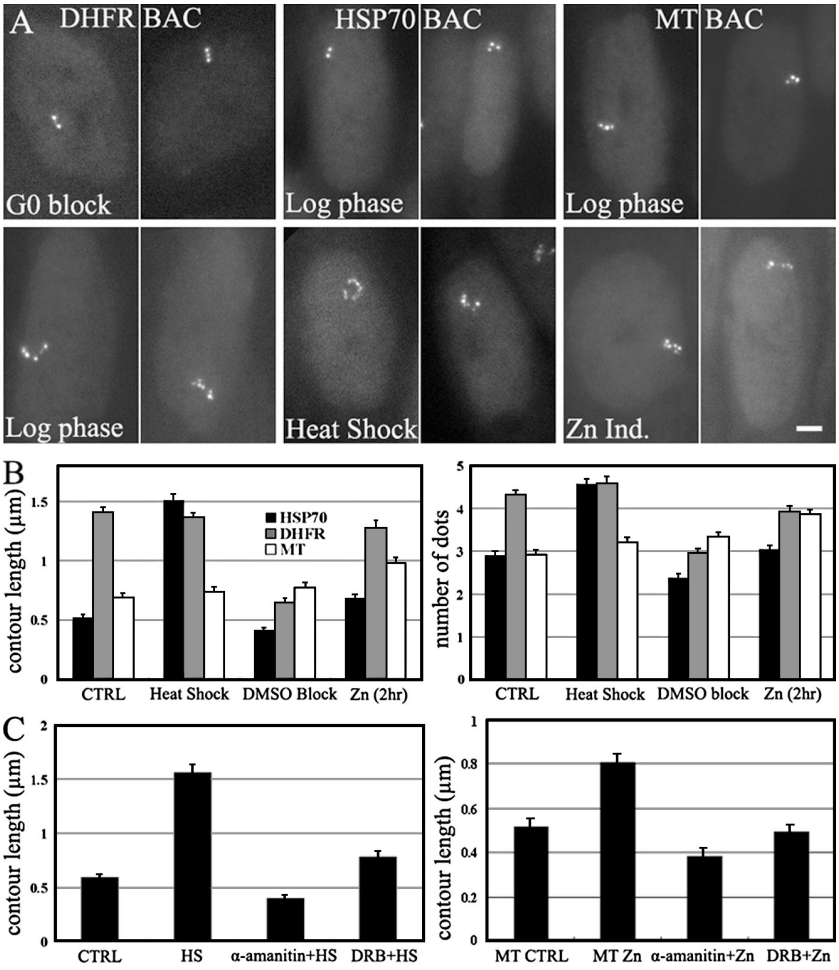

Figure 2. **Large-scale chromatin decondensation accompanies gene activation.** (A) GFP-lac repressor fluorescence before (top) and after (bottom) gene induction for the DHFR (057L22), Hsp70, and MT BACs. After induction, a more extended "string of dots" is observed. Bar, 2 μm. (B) Histograms showing mean contour lengths (left) or GFP spot number (right) for each BAC cell line at normal growth conditions (CTRL) (DHFR gene induced) and after heat shock (Hsp70 genes induced), Zn addition (MT genes induced), or DMSO induced G1 arrest (DHFR repressed) (see text). Increases in contour length and spot number are specific for the induction conditions appropriate for the particular BAC transgene. (C) Histograms showing contour length under CTRL or induced conditions for Hsp70_5 and MT1_1_4 cell lines with and without transcriptional inhibition. Chromatin decondensation accompanying heat shock is blocked by α-amanitin and significantly reduced by DRB (see text). (B and C) Histogram data points are based on > 100 cells (SEM error bars).

might be forming more highly decondensed DNA loops protruding outwards from a highly condensed, large-scale chromatin "backbone" containing the lac operator repeats. Lac operator repeats were located 64, 25, 37, 4, and 35 kb away from the DHFR, HspA1A, HspA1B, MT1A, and MT2A genes, respectively (Fig. 1 B). However, for the DHFR BAC, the lac operator repeat is inserted within the Msh3 gene, expressed from the same divergent promoter as DHFR and showing similar cell cycle expression (Farnham and Schimke, 1986; Schilling and Farnham, 1995). For the MT BAC, the lac operator repeat is inserted within a cluster of MT1 genes, ubiquitously expressed in various tissues (Hidalgo and Carrasco, 1998). Thus, in both these BACs, the lac operator repeat is inserted within regions likely to be transcriptionally active.

However, to more rigorously test this possibility, we used two-color, 3D DNA FISH on DHFR and Hsp70 BAC transgene arrays to localize the signal from the lac operator repeats relative to the BAC FISH signal. The lac operator FISH probe produced a spot-like pattern very similar to GFP-lac repressor binding in the same cell lines (Fig. 2 A), frequently forming a linear trajectory. To best visualize the spatial relationship between lac operator and BAC FISH signals, we focused on cells with highly extended BAC transgene arrays with a large number of lac operator spots (Fig. 3). Lac operator probe (red) spots generally coincided and were co-linear with similar FISH signals from the BAC probe (green) with no evidence for looping of BAC sequences a significant distance away from a linear backbone (Fig. 3).

We also examined a different stable cell line (110–5-E4) created from the shorter DHFR BAC (560M7-K8.32-C-5, Fig. 1 B) in which the lac operator repeat is inserted directly into the fifth DHFR intron. The configuration of GFP spots in this cell line looked very similar to that observed in the DHFR D10 BAC cell line, frequently lining up in a linear trajectory (Fig. 3 B). Co-linear lac operator and BAC FISH signals for the Hsp70_5 cell line were also observed (Fig. 3 C).

Using a new, in vivo immunogold labeling procedure, we also visualized by EM the location of the lac repressor stained operator repeats relative to chromatin in DHFR D10 cells. Consistent with the 3D FISH results, lac repressor spots localized within condensed, large-scale chromatin structures (Fig. 3 D).

Large-scale chromatin decondensation is blocked or significantly reduced after transcriptional inhibition

To investigate whether transcription is required for decondensation, we treated cells carrying the Hsp70 or MT BACs with two different transcriptional inhibitors: α-amanitin and 5,6-dichloro-1-β-D-ribobenzimidazole (DRB). α-Amanitin specifically inactivates and targets the RNA polymerase II largest subunit for rapid degradation (Nguyen et al., 1996), whereas

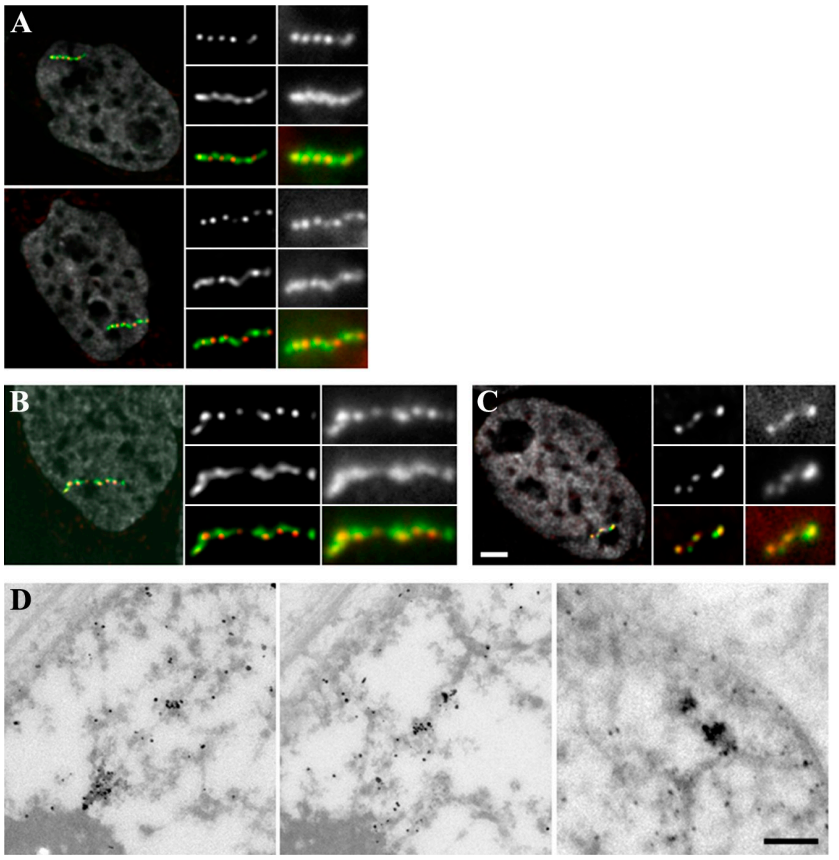

Figure 3. **No evidence for extended looping of BAC sequences from a linear backbone.** (A–C) 3D DNA FISH shows co-linear signals from the Lac operator (red) and BAC (green) probes. DNA is stained by DAPI (gray). (A) DHFR D10 cells. (B) DHFR-110-5-E4 cell with lac operator repeats inserted into the DHFR gene fifth intron. (C) Hsp70_5 cell 30 min after heat shock. Middle columns (deconvolved data) and right columns (raw data) show 2x enlarged views (Bars, 2 μm). (D) EM of DHFR D10 clone by in vivo immunogold staining of EGFP-LacI shows the BAC transgenes are compacted indistinguishable from surrounding genomic DNA, with no obvious looping structure from the transgene backbone. Left and middle: serial sections (150 nm); right: 500-nm section (Bar, 500 nm).

the transcription inhibitory effects of DRB may be related to interference with the activity of the CTD kinase and therefore transcriptional elongation (Dubois et al., 1994).

With α-amanitin treatment, both the Hsp70 and MT transgene arrays after transcriptional induction became slightly more condensed (shorter contour lengths) than that observed in noninduced control cells (>99% confidence level). This may be related to inhibition of constitutive transcription levels (Fig. 2 C), although we cannot exclude general effects induced by global transcriptional inhibition on nuclear and/or chromosome structure. In DRB treated cells, the Hsp70 transgene array showed a statistically significant decondensation (>99% confidence level) after heat shock, but the magnitude of this decondensation was significantly reduced relative to cells not treated with DRB (>99% confidence level). For the MT transgene array, no statistically significant difference in contour lengths was observed between noninduced control cells versus Zn induced DRB treated cells. Hsp70 is known to have a poised polymerase (Price, 2008). The differential decondensation observed with these two inhibitors therefore might be related to the presence or absence of RNA polymerase at the Hsp70 promoter, with DRB treatment still leaving a poised polymerase at the Hsp70 promoter and allowing initiation of transcripts after heat shock.

Transcriptional activation occurs for most BAC copies but gene and BAC sequences remain co-linear

On average the BAC transgenes are expressed within several fold of the endogenous genes (Table II). This could occur either through a reduced transcription rate at each transgene copy or through a normal transcription rate at a small fraction of BAC transgenes. In the latter case, our previous observations would not be informative with regard to the relationship between active transgene expression and large-scale chromatin compaction.

Using RNA FISH, we asked roughly what fraction of BAC transgene copies were active within the transgene arrays, focusing on DHFR and Hsp70 BAC cell lines. RNA FISH signals using the entire BAC as a probe were found adjacent and/or partially overlapping most GFP spots in both DHFR BAC transgene cell lines (Fig. 4, A and B). Similarly, RNA FISH signals, detected using the HspA1A gene as a probe, also were close to or overlapping with most GFP spots at early times (5–10 min) after heat shock in the Hsp70 BAC transgene cell line (Fig. 4 C).

We assumed the increased separation of RNA FISH versus GFP-lac repressor signals, as compared with lac operator versus BAC DNA FISH signals (Fig. 3), reflected transcript accumulation away from the actual sites of transcription (for review see Johnson et al., 2000). Indeed dual DNA FISH showed excellent colocalization between DHFR gene and total BAC probes (Fig. 4, D and E). The short, ∼2-kb Hsp70 gene sequences were detected using tyramide signal amplification (TSA) (Fig. 4 F). Again increased colocalization was observed in most regions relative to the RNA FISH results. A minority of Hsp70 signals did not overlap with BAC hybridization, but because these were co-linear with nearby BAC signals we interpret their lack of overlap with gaps created by incomplete BAC hybridization, compounded by the much higher detection sensitivity of the TSA Hsp70 gene detection (Fig. 4 F). However, we cannot exclude a more extensive decondensation in the neighborhood of some transcribed Hsp70 genes.

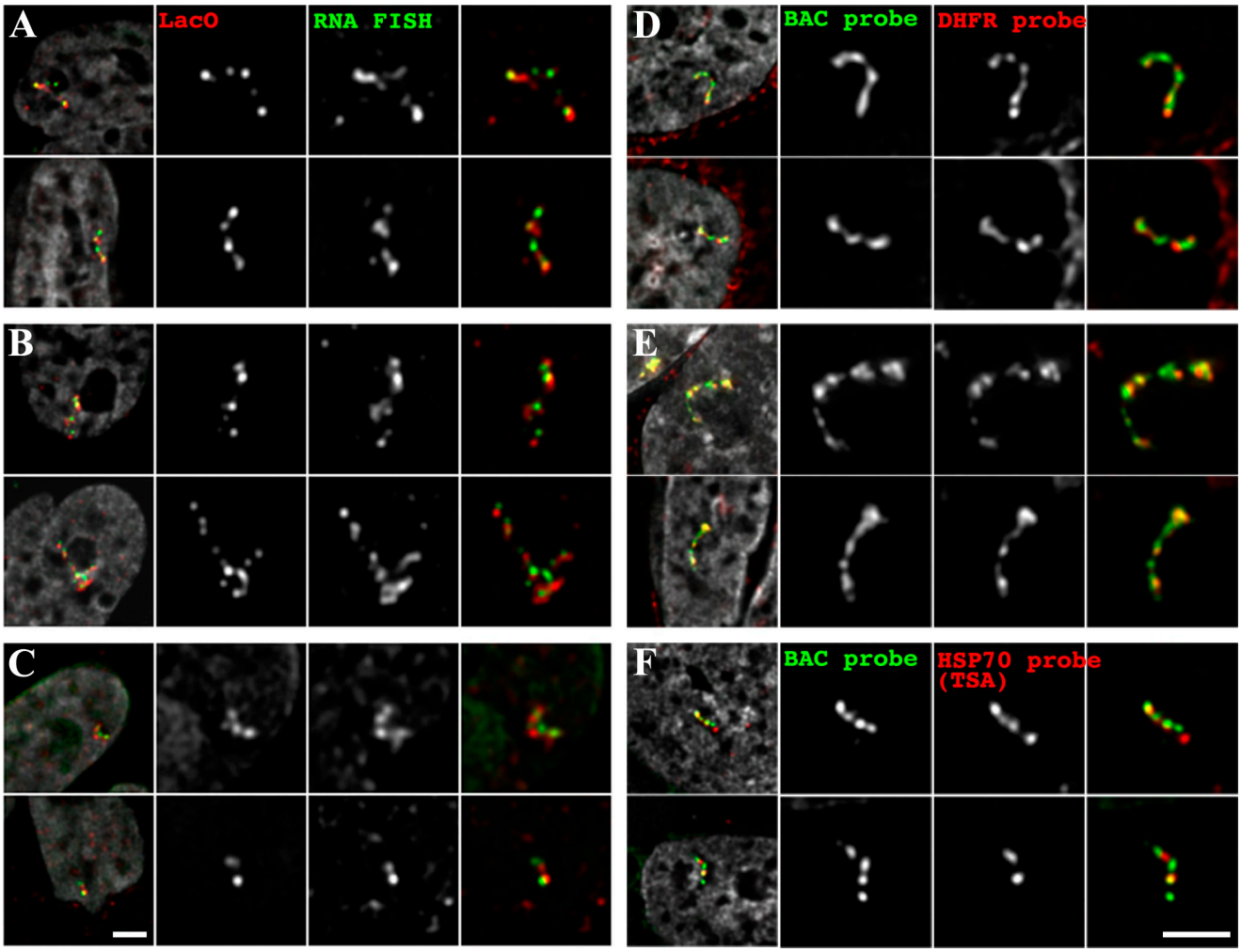

Figure 4. **Most BAC transgene copies are transcriptionally activated with gene sequences co-linear with BAC sequences.** (A–C) RNA FISH (red) shows DHFR BAC and Hsp70 gene transcripts relative to GFP-lac repressor (green) after gene induction. DNA is stained by DAPI (gray, left column). (A and B) Log phase cells with DHFR BAC transgenes showing RNA FISH using the entire BAC as probe. (A) D10 cell line with 057L22-K-8.32-C29 DHFR BAC containing lac operator repeats inserted 64 kb upstream of the DHFR gene. (B) 110–5-E4 cell line with 560 M7-K-8.32_C5 DHFR BAC containing lac operator repeats inserted into the DHFR gene fifth intron. (C) Hsp70_5 cell line 5 (top) or 10 (bottom) mins after heat shock induction using Hsp70 transcribed region as RNA FISH probe. RNA FISH signals are adjacent or partially overlapping with GFP signals in all three cell lines. (D–F) DNA FISH reveals actual localization of transcribed gene sequences relative to overall BAC sequence. Co-localization is much more extensive than that observed with RNA FISH and co-linear with the linear BAC signals. (D and E) Pooled PCR probes covering most of DHFR gene (red), total BAC sequence (green) in D10 (D) or 110–5-E4 (E) cells. (F) Hsp70_5 cell line 30 min after heat shock. Approximately 2 kb Hsp70 gene probe (red) localized used tyramide amplification method, relative to directly labeled BAC probe (green). Bar, 2 μm.

Our previous measurements (Fig. 2) suggested an average of 2–3 BAC transgene copies per GFP spot for induced transgenes. Some GFP spots have lower intensity than others, suggesting a variable number of BAC copies, and therefore a differential overall large-scale chromatin compaction per spot. However, RNA FISH signals were observed independent of the brightness of adjacent GFP spots (Fig. 4). Therefore, transcription activation occurs for most individual BAC copies independent of differential large-scale chromatin compaction. RNA FISH reveals Hsp70 transgene expression begins in >90% of cells within 5 min of heat shock whereas large-scale chromatin decondensation increases from 10–30 min after heat shock (Fig. S3).

Hsp70 transgenes associate with nuclear speckles after heat shock

Transcriptionally active BAC transgenes showed a several fold average decondensation of large-scale chromatin structure, with the more highly decondensed examples showing extended, linear conformations for the DHFR and MT genes (Figs. 2–4). In contrast, at 30 min after heat shock a significant fraction of Hsp70 transgenes showed a unique, semi-circular conformation not observed for DHFR or MT BAC transgenes (Fig. 2 A). Moreover, whereas RNA FISH showed good colocalization of GFP spots with Hsp70 transcripts at short times after heat shock (Fig. 4 C), at later times Hsp70 transcripts accumulated within a DAPI poor hole encircled by the GFP spots (Fig. 5 A).

This impression was confirmed by a strong association of the Hsp70 BAC transgenes, but not DHFR or MT transgenes, with SC-35 or ASF/SF2 immunostained speckles (Fig. 5, B and C). Analysis of several independently derived cell lines from each of the three BACs revealed this speckle association in all of the Hsp70 BAC transgene cell lines but none of the DHFR or MT BAC cell lines, indicating that this association was specific to the Hsp70 transgene rather than the chromosome integration

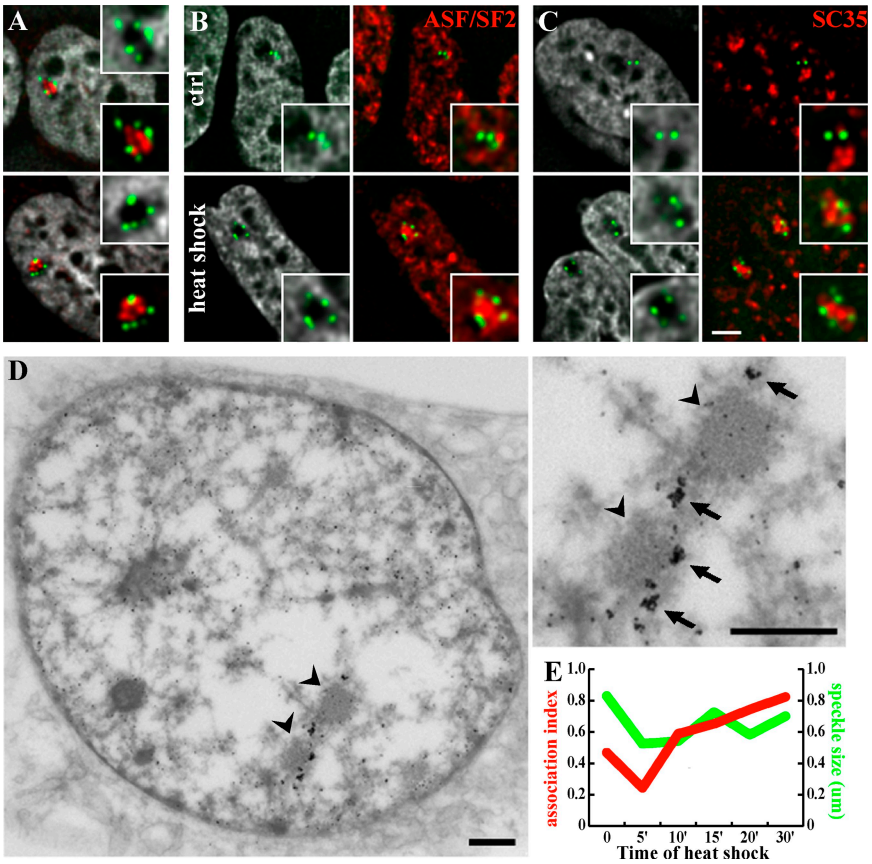

Figure 5. **Hsp70 transgenes associate with nuclear speckles after heat shock.** (A) Hsp70 transcripts, detected by RNA FISH (red), accumulate within a DAPI (grayscale) poor region encircled by GFP-LacI signals (green) marking the Hsp70 transgene locations. (B and C) Close association of Hsp70 BAC transgenes, marked by EGFP-LacI (green), with nuclear speckles immunostained either with ASF/SF2 (B) or SC35 (C) antibodies (red) in Hsp70_5 cells 30 min after heat shock (bottom panel) as compared with nonheat shocked control cells (top panel). Grayscale shows DNA staining (DAPI). Bar (A–C), 2 µm. (D) In vivo immunogold staining of EGFP-LacI marks transgene location (arrows) associated with IGC (nuclear speckle). Enlarged area (right) shows that transgenes appear at the periphery of the dense cluster of granules defining the IGC (arrowheads). Bar, 1 µm. (E) Comparison of the diameter of the nearest nuclear speckle (average of longest and shortest speckle axes, green) versus transgene association index (red, see text) at different times after heat shock. Transgene association index increases from 50–90% during heat shock with no major change in average size of nearest speckle.

site (unpublished data). In vivo immunogold labeling of the Hsp70 BAC transgene revealed localization of the lac operator tag to the periphery of interchromatin granule clusters (IGC)—specifically to the amorphous/fibrillar material surrounding the dense central, granular core (Fig. 5 D). Combined immunofluorescence and RNA FISH confirmed that Hsp70 transcript accumulation was occurring within SC-35 stained speckles at later times after heat shock (unpublished data).

Accumulation of transcripts within SC-35 speckles from genes associated with these speckles has been described previously (Johnson et al., 2000; Smith et al., 2007). This association of Hsp70 BAC transgenes with nuclear speckles/IGCs mirrors the previously reported association of the endogenous Hsp70 gene with nuclear speckles, with speckle association increasing from 10% to 90% after heat shock (Jolly et al., 1999). We defined the association index as the fraction of GFP spots in close contact with the edge of an SC-35–labeled speckle. In this cell line, the association index increased from 47% to 85% between 0 and 30 min after heat shock, whereas the average size of the nearest speckle remained relatively stable (Fig. 5 E), suggesting that Hsp70 transgenes might simply move closer to preexisting speckles.

Dynamics of Hsp70 transgene and nuclear speckle association

To address more directly how Hsp70 transgenes associate with nuclear speckles after heat shock, we performed live-cell imaging. Previous live-cell imaging of GFP-ASF/SF2 dynamics during activation of a viral transgene suggested recruitment of splicing factors to the viral transgene through a local protrusion from a nearby nuclear speckle (Misteli et al., 1997); in this study the location of the viral transgene was revealed only at the end of the observation period after fixation and FISH. Increased speckle association of Hsp70 transgenes after heat shock could occur through several distinct processes: (1) nucleation of new speckles near the transgene; (2) enlargement of a preexisting, nearby speckle; (3) transgene movement toward a speckle; (4) speckle movement or protrusion toward the transgene.

To distinguish among these possibilities, we developed a stable cell line coexpressing mRFP-ASF/SF2 and GFP-dimer lac repressor (Hsp70_5_P9_4). The mRFP fluorescence pattern was nearly identical to the immunofluorescence staining using anti-SC35 or anti-ASF/SF2 antibodies. Western blot analysis showed expression levels of mRFP-ASF/SF2 were approximately one fourth endogenous ASF/SF2 protein levels (unpublished data). Live-cell imaging revealed examples of the first three possibilities outlined above. Most frequently we observed nucleation of new splicing speckles adjacent to transgenes or enlargement of a preexisting nearby speckle, but in rare cases long-range movement of transgenes toward SC-35 speckles was observed (Fig. 6).

Previous work examining chromosome movement in response to transcription factor tethering had revealed a pronounced photosensitivity of long-range chromosome movement (Chuang et al., 2006). Due to technical limitations of our microscope system and the expression levels of the GFP and mRFP fusion proteins, exposure times required in these Hsp70/speckle live experiments exceeded the threshold at which inhibition of long-range chromosome movement previously was observed. In fact,

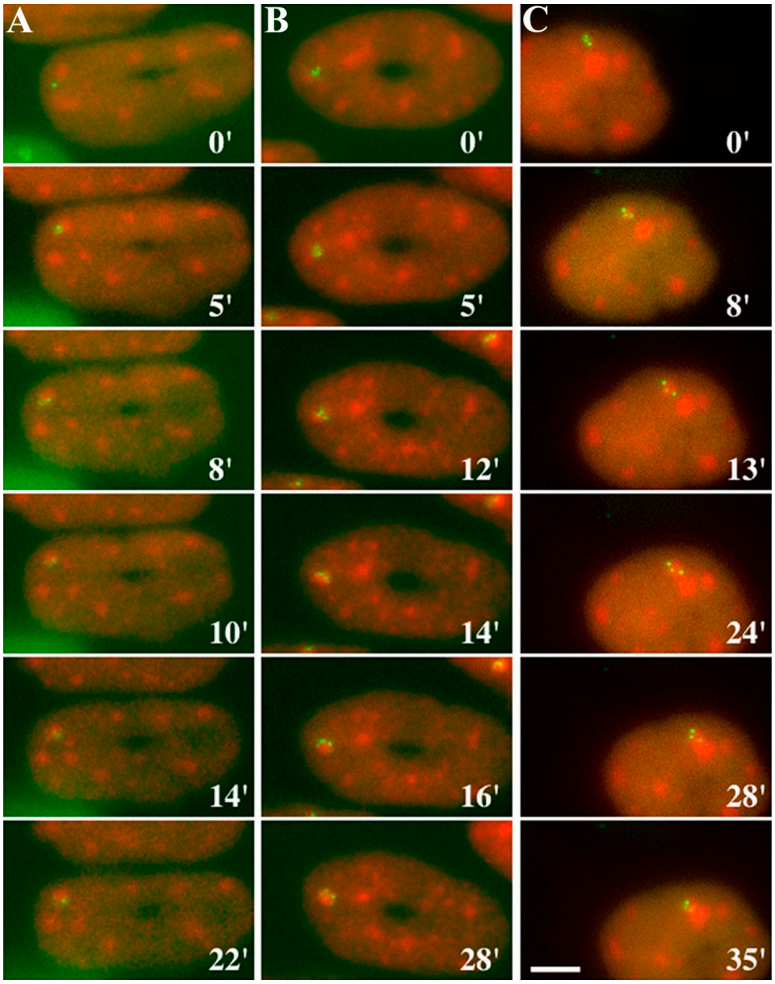

Figure 6. **Live imaging shows three possible transgene/speckle dynamic events during heat shock.** (A) Long-range movement of Hsp70 BAC transgenes (green) toward a ASF/SF2 speckle (red) occurred within a 5-min heat shock period (Video 1). (B) Enlargement of preexisting speckle together with decondensation and increased association and encircling of BAC transgenes around speckle exterior (Video 2). (C) Nucleation of a new ASF/SF2 speckle adjacent to the Hsp70 BAC transgenes several minutes after heat shock; newly nucleated speckle then merges with preexisting adjacent speckle forming a larger speckle (Video 3). Bar, 5 μm.

the few examples of long-range chromosome movement observed here involved movement within the first few time points. It is therefore possible that long-range movements occur more frequently; experiments beyond the scope of the current study are now in progress to investigate this possibility.

Seen frequently is a relatively early movement of the neighboring GFP spots, initially not in contact with an adjacent, preexisting speckle, to the speckle periphery (Fig. 6 A; Video 1). GFP spots appear to encircle the edge of the speckle as the BAC transgene array decondenses (Fig. 6 B; Video 2). Interestingly, in all live experiments GFP spots showed a strong tendency to remain associated with the speckle periphery, versus becoming engulfed within a growing speckle. In one example in which two speckles merged, GFP spots that appeared transiently within the merged speckle moved back to the periphery of the merged speckle (Fig. 6 C; Video 3).

Active genes remain mobile without stable attachments to nuclear structure

Previous live-cell imaging has revealed a rapid but locally constrained movement of lac operator tagged chromosome sites in a variety of cell types, including mammalian cells (Marshall et al., 1997; Heun et al., 2001; Vazquez et al., 2001; Chubb et al., 2002). This includes individual GFP spots from the B9 CHO cell line containing the 057L22-K-8.32-C29 DHFR BAC (Levi et al., 2005). Because all of these studies monitored the motion of individual spots, two spots on different chromosomes, or two spots on opposite ends of a large BAC transgene array separated by several micrometers, the actual origin of these movements has not been clear. This motion has usually been conceptualized as diffusion of a chromosome locus tethered to a nearby nuclear structure. An alternative explanation could be local deformations or movements of a nuclear subregion.

Here we used direct live-cell imaging to visualize the movements of all GFP spots within the DHFR BAC transgene array in B9 cells relative to each other. Although a detailed analysis of motion is beyond the scope of this study, a simple observation emerged. Similar rapid but constrained movement of the DHFR BAC transgenes over a time scale of seconds (Fig. 7; Video 4) is observed. Because multiple spots, corresponding to a co-linear, integrated BAC array move relative to each other while maintaining their co-linear arrangement, this demonstrates that the observed movement is not due to a local movement of the entire chromosome region or the movement of an entire nuclear subvolume. Rather, these movements correspond to local movements or conformational changes of a several hundred kb chromatin region relative to flanking cis sequences.

RNA FISH revealed that nearly all GFP spots in the DHFR BAC transgene arrays overlap or are adjacent to transcripts under induced conditions (Fig. 4), implying that most BAC transgenes

are active. Assuming a 50-bp/s transcription rate, the DHFR gene should require more than 10 min for complete transcription. Our results showing GFP spots in motion relative to each other on a much faster time scale, with each spot on average containing ~2 BAC copies, appear to contradict models in which transcription occurs on a solid nuclear matrix or transcription body anchored to a static nuclear scaffold. We cannot exclude movement of a mobile nuclear scaffold within the transcribing transgenes.

Discussion

For many years, the looped domain model for interphase chromatin structure has represented our foundation for conceptualizing in vivo gene transcription, with a resulting emphasis on understanding basic questions derived directly from this model. This looped domain model, however, is based heavily on the cytology of atypical genes. In lampbrush chromosome loops (Spring and Franke, 1981) and some insect polytene puffs (Olins et al., 1986; Bjorkroth et al., 1988), DNA is decondensed to below the level of a nucleosome in areas of unusually high RNA polymerase density. In contrast, the average, pol II transcribed gene in somatic, diploid nuclei has less than one engaged RNA polymerase per transcriptional unit (Jackson et al., 2000). Moreover, in the case of the Balbiani ring puff, transcription inhibition results in a lowered density of engaged RNA polymerases and rapid chromatin refolding—a 10-nm nucleofilament segment near the last engaged polymerase can be seen to transition within a short distance into a 30-nm chromatin fiber (Andersson et al., 1982).

Visualizing the actual conformation for typical RNA pol II genes within diploid nuclei has been highly problematic, not only because of the inherent resolution limit of light microscopy but also because of uncertain structural preservation after the harsh DNA denaturation conditions used with FISH.

Here we have set out to overcome both problems, first by building a repeating transgene array large enough to readily detect small changes in conformation by light microscopy, and second by using a protein/DNA tag to allow preservation of structure while permitting direct in vivo visualization and immunogold ultrastructural visualization. In this third generation approach, we have used large cloned genomic loci surrounding specific inducible genes, reconstituting transgene expression levels within several fold of the corresponding endogenous genes.

Our results demonstrate a 400–1,000-fold average compaction ratio after gene induction, well above the ~30–40-fold compaction ratio of 30-nm chromatin fibers. Such high compaction ratios suggest folding of 10- and 30-nm chromatin fibers into highly condensed large-scale chromatin fibers, consistent with our light and electron microscopy data, rather than reflecting merely a somewhat sinuous versus straight path of isolated 30-nm chromatin fibers. In examples where the number of GFP/lac operator spots is close to the BAC copy number, DNA FISH reveals an extended, linear fiber several microns in length with lac operator arrays punctuating the more continuous signal from the BAC probe. Even in these maximally extended examples the compaction is more than fourfold higher than the 30-nm chromatin fiber, with no evidence for an extended loop model. We assume that there must be some local chromatin decondensation,

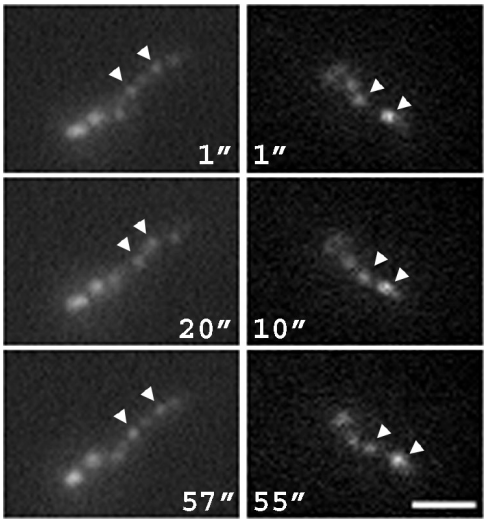

Figure 7. **Rapid movement of DHFR BAC transgenes along the transgene array axis implies chromatin conformational changes over a several second time scale.** Live-cell imaging of DHFR BAC B9 cell line with ~1-s time intervals (Video 4). Two examples (left and right) show GFP spots moving relative to each other (arrowhead) along the direction of the BAC transgene array chromosome axis. Video 4 shows most GFP spots are in rapid motion relative to each other on a time scale far shorter than the estimated 10 min required for complete transcript synthesis, implying the absence of stable attachments of transgenes to surrounding nuclear structures during transcription. Bar, 2 µm.

not detectable with our imaging approaches, immediately surrounding the polymerase during transcription, and we cannot rule out DNA loops smaller than the gene which are not detectable by FISH. How large such decondensed regions might be and whether the polymerase tracks along DNA within the large-scale chromatin fibers or remains at the periphery in a "transcription factory" remains to be determined.

For DHFR and Hsp70 BAC transgenes the average number of GFP spots in the induced state was approximately half the number of BAC copies, suggesting transcription at even higher compaction levels than indicated by the average large-scale chromatin compaction values. The origin of this nonuniform compaction observed in these more typical cases is not clear. Similar "beaded" conformations in human cells were observed for two ~400-kb, trancriptionally active regions as assayed by DNA FISH (Muller et al., 2004), although we cannot exclude effects related to pairing of lac operator repeats as observed in *Arabidopsis* for lac operator repeats separated by as much as 5 Mbp (Pecinka et al., 2005). However, unlike the *Arabidopsis* example, no evidence for looping out of intervening DNA was observed by FISH, with both BAC and lac operator DNA contained within the more condensed foci in these CHO cells.

The overall large-scale compaction observed was quite similar for all BAC cell lines examined, particularly when comparing induced versus noninduced transcription states. We assume that the very large size of the multi-copy BAC insertions (~2 Mbp in this study) helps shield these sequences from influences from flanking chromosome regions. Moreover, the similar relative changes in BAC transgene compaction for the different BAC cell lines as a function of transcriptional induction, despite very different levels and ratios of constitutive and induced transcription for the three

BAC transgenes, argues that the amount of decondensation is not determined simply by the level of transcription.

Interestingly, the ~1,000-fold compaction ratio observed for a heterochromatic transgene array after targeting of the VP16 acidic activation domain (AAD) (Tumbar et al., 1999) is nearly the same as we observed before transcriptional induction of the DHRF and Hsp70 BAC transgenes. The magnitude of the previously described dramatic unfolding of heterochromatin transgene arrays induced by the VP16 AAD likely reflects epigenetic remodeling of heterochromatin, rather than transcriptional activation of genes contained within euchromatin, by itself. The modest, ~2–3-fold decondensation with transcriptional induction for these BAC transgenes is likely to be more representative of changes in large-scale chromatin conformation associated with inducible genes embedded in euchromatin.

Transcription of the Hsp70 transgene is detectable by RNA FISH 5 min after heat shock, whereas average large-scale chromatin decondensation over the BAC transgene array increases 10–30 min after heat shock. Therefore, long-range, large-scale chromatin decondensation is unlikely to be required for transcriptional activation, by itself, but may have a quantitative effect on transcription levels, as Hsp70 RNA FISH signals are smaller and weaker in intensity at 5 min as compared with later times after heat shock. A more direct test of the exact casual relationship between large-scale chromatin compaction and transcription will require more sophisticated, live-cell experiments.

Large-scale chromatin decondensation may depend on transcription, and/or factors recruited by the RNA polymerase holoenzyme, as inhibition of transcription greatly reduced or eliminated decondensation. This is different from the previously observed large-scale chromatin decondensation induced by VP16 AAD targeting to a heterochromatin region which was only partially reduced by the same treatments.

In certain cell types, genes have been reported to associate within minutes of transcriptional activation with relatively large nuclear foci, or transcription factories, which stain for high levels of RNA polymerase 2 (Osborne et al., 2004). In fibroblasts, as well as cell lines such as CHO and HeLa, comparably sized foci are not observed. Instead thousands of smaller transcription factories are observed by BrUTP staining. Because the number of these sites is still smaller than the estimated number of active genes, these foci have been proposed to correspond to the clustering of active genes (Iborra et al., 1996). However, in these cells in which large transcription factories are not observed, what has been observed is clustering of gene rich chromosome regions and a significant fraction of individual genes with relatively large nuclear bodies called IGCs, or nuclear speckles, enriched with splicing factors (Shopland et al., 2003).

For the DHFR and MT BAC transgenes, we saw no evidence for increased clustering of active transgenes after gene induction, which might be expected in a model in which active genes in cis would colocalize to the same, large transcription factory. Instead, we saw an increased number of GFP spots and an increased extension of large-scale chromatin fibers with gene induction for these BAC transgenes.

We did, however, see a clear curvilinear folding of Hsp70 transgenes correlating with increased association of Hsp70 BAC transgenes with IGCs rather than transcription factories, reproducing the known association with IGCs of the endogenous Hsp70 locus after heat shock (Jolly et al., 1999). Light microscopy of fixed and live-cells localizes these genes nearly always to the periphery, rather than interior, of the IGC, with ultrastructural localization of the Hsp70 transgenes to the diffuse fibrillar material surrounding the granular core of the IGC. To our knowledge our results represent the first ultrastructural visualization of the association of specific, active genes with IGCs. Work is now in progress to dissect what cis elements are required for speckle association.

Our use of the lac operator/repressor labeling system allowed direct, live-cell imaging of BAC transgene large-scale chromatin dynamics. The observed rapid motion, including movement of individual spots in directions parallel to the linear path outlined by adjacent spots, provides the first direct data supporting the local conformational fluctuations, or "breathing", of large-scale chromatin fibers occurring on the same time scale of previously described movements of isolated chromosome foci, previously conceptualized as "constrained diffusion". Our results suggest movement of much of the transcriptional machinery with the chromatin, with any local anchoring to nuclear structures likely to be transient; if stable loop attachments are present they are likely to be internal, associated with other parts of the surrounding interphase chromatid.

Using live-cell imaging, we also provide the first direct visualization of how active genes become associated with IGCs or nuclear speckles. Several different scenarios were observed, including movement of the transgene to a speckle, nucleation of a new speckle adjacent to the transgene, or enlargement of a preexisting speckle adjacent to the transgene. Further studies beyond the scope of this current paper with introduction of improved technology to reduce phototoxicity will be required to determine the relative frequencies of these different scenarios and, in particular, whether the motion of the BAC transgene occurs via directed movements, as described recently for two specific examples of interphase chromosome movements (Chuang et al., 2006; Dundr et al., 2007).

Overall, our results demonstrate a tight correlation between long-range, large-scale chromatin decondensation of a euchromatic chromosome region and transcriptional activation from constitutive to induced levels. However, decondensation is not absolutely required for transcription, while transcription by itself, or at least components of the transcriptional machinery, may be required for large-scale chromatin decondensation. The major future challenge will be in extending this system to address whether long-range chromatin decondensation, and/or association with nuclear bodies such as IGCs, is causally related not to transcription, per se, but to increased transcriptional activity and/or fine-tuning of transcriptional regulation.

Materials and methods

Vector construction and BAC modification

The mRFP fragment was excised from pRSETB using NdeI, blunt-ended, cut with HindIII, and ligated into vector p3′SS-EGFP-dimer_LacI-VP16, cut with Eco47III and HindIII, creating p3′SS-mRFP-VP16. The vector pmRFP was created by linearizing p3′SS-mRFP-VP16 with BamHI which was blunt-ended and then cut with HindIII, generating an mRFP fragment which was inserted into pEGFP-C1 (Clontech Laboratories, Inc.) cut with Eco47III and HindIII. The mouse ASF/SF2 cDNA (American Type Culture Collection; mouse 5708288 pYX) was PCR amplified (forward, 5′-CGCGGATCCTGTACGAGAGCGAGATCTGCT-3′;

reverse, 5′-CCGGAATTCATGTCGGGAGGTGGTGTGATC-3′) and cloned into the BamHI, EcoRI sites of pmRFP, creating pmRFP_ASF/SF2, expressing mRFP-ASF/SF2 from a CMV promoter. The puromycin resistance gene was excised using PvuII and BamHI from pPUR (BD Biosciences, Clontech), blunt-ended, and ligated with the blunt-ended fragment from pmRFP-ASF/SF2, cut with MluI.

To create Tn5 transposons, the pSP2 (Carpenter and Belmont, 2004) polylinker was modified by insertion of adaptor (AATTGACAGCTGTC-GATC) containing a PshAI/PvuII site between the EcoRI and BamHI sites, creating pPvuII. Tn5 transposon "Kan-2" (Epicentre Technologies) was inserted into the pPvuII site, creating p[Kan]. A Kan/Neo cassette was PCR amplified from pECFP-C1 (BD Biosciences Clontech) (forward, 5′-CGG-GATCCATTCAAATATGTATCCGCT-3′; reverse, 5′-CGGAATTCGTTTAT-GAACAAACGACCCAAC-3′) and inserted into pMOD-2 (Epicentre Technologies) between the BamHI and EcoRI sites. p[Kan/Neo] was created by excising from this plasmid the Kan/Neo cassette flanked by Tn5 mosaic ends using PshAI and ligating it into p[Kan], replacing the KanR cassette, excised with PshAI. The 8.32 lac operator repeat was cut out of pSV2-DHFR-8.32 (Robinett et al., 1996) using a SalI and XhoI digest and inserted into p[Kan] or p[Kan/Neo] linearized with SalI to create p[Kan-8.32] or p[Kan/Neo-8.32].

Dihydrofolate reductase (DHFR) bacterial artificial chromosome (BAC) clones 057L22 and 560M7 were obtained from the CITB mouse library and are based on the pBeloBac11 vector; Hsp70 BAC clone 92G8 and Metallothionein (MT) BAC clone 134B2 from the RPCI-11 human library are based on the pBACe3.6 vector. Transposition of the p[Kan-8.32] transposon into the DHFR BACs and the p[Kan/Neo-8.32] transposon into the Hsp70 BAC and MT BACs used the EZ::TN <KAN-2> Insertion kit (Epicentre Technologies) following the manufacturer's instructions. Transposon insertion sites were mapped by DNA sequencing from both transposon ends: 64 kb 5′ to the DHFR locus in the 057L22-K-8.32-C29 clone, within the fifth intron for the 560 M7-K-8.32_C5 clone, 20 kb 5′ to the Hsp70 locus in the 92G8-K/N-8.32_C2 clone, and inside the MT locus (35 kb upstream of the MT2A gene) in the 134B2-K/N-8.32_C8 clone.

Cell culture and establishment of BAC cell lines

CHO DG44 cells with a double deletion of the endogenous DHFR locus (Urlaub et al., 1986) were incubated at 37°C with 5% CO_2 in Ham's F12 media (Invitrogen) plus 10% FBS (Hyclone). CHO DG44 cells (Clone 7) stably expressing EGFP-dimer lac repressor (Tumbar et al., 1999) were used for all BAC transfections. Circular BAC DNA was transfected using Fugene6 (Roche) according to the manufacturer's directions. Stable cell clones containing DHFR BACs were selected in F12 media without thymidine and hypoxanthine (Invitrogen) and with 10% dialyzed FBS (Hyclone). The Hsp70 and MT BAC transgene cell lines were selected in 200 µg/ml G418 in F12 media supplemented with 10% FBS. Stable transformants were subcloned by serial dilution.

Mitotic chromosome examination

Logarithmically growing cells were arrested with 200–600 ng/ml nocodazole in fresh media for 2 h. Mitotic cells were collected by shake-off, centrifuged in media onto poly-L-lysine–coated coverslips at 4°C, fixed in 1.6% formaldehyde (Polysciences) in PBS buffer for 30 min at RT, and stained with DAPI. Methanol/acetic acid–fixed mitotic chromosome spreads were prepared according to standard cytogenetic procedures (Beatty and Scherer, 2002).

DNA probe preparation

BACs, pSV2-DHFR-8.32 (lac operator 256mer repeat) (Robinett et al., 1996), and HSPA1A and DHFR gene PCR products (primers in Table S3) were biotin labeled by nick translation (BioNick kit; Invitrogen) according to the manufacturer's instructions. Alternatively, the biotin-labeled nucleotide mix in the kit was substituted with the digoxigenin nucleotide mix (0.5 mM dATP, dGTP, and dCTP, 0.375 mM dTTP (Invitrogen), 0.125 mM DIG-dUTP (Roche), 0.5 M Tris-HCl pH 8.0, 0.5 mg/ml BSA (Sigma-Aldrich), and 50 mM $MgCl_2$) for digoxigenin labeling.

3D DNA FISH

Cells on coverslips were fixed using freshly prepared 4% paraformaldehyde in calcium, magnesium-free PBS (CMF-PBS) for 10 min at RT followed by permeabilization in CMF-PBS using 0.5% Triton X-100. Coverslips were placed in 20% glycerol/CMF-PBS for 30 min, subjected to four freeze-thaw cycles using liquid nitrogen, then immersed in 0.1M HCl for 7.5 min before storing in 50% deionized formamide (Sigma-Aldrich)/2xSSC as described elsewhere (Solevei et al., 2002). 2 µl of hybridization mix (50 ng/µl probe concentration in 50% deionized formamide, 10% dextran sulfate, 2X SSC) was applied before mounting coverslips to glass slides using rubber cement. Denaturation at 75°C for 2 min on a heat block was followed by hybridization overnight at 37°C in a humidified chamber, followed by washes in 0.4X SSC at 70°C for 2 min and SSCT (2xSSC/0.2% Tween 20) at room temperature. Detection used Strepavidin-Alexa 594 (1:200; Invitrogen) or anti-DIG-fluorescein antibodies (1:200; Roche) in 4% BSA/SSCT.

RNA FISH

RNA FISH and RNA FISH combined with immunostaining procedures were performed as previously described (Chaumeil et al., 2004) with using Streptavidin-Alexa 594 (1:200; Invitrogen) in 1% BSA/4xSSC/2 mM vanadyl ribonucleoside complex (VRC; New England Biolabs, Inc.).

Transgene copy number analysis

BAC transgene copy number estimates were determined for three cell lines (DHFR D10, HSP70_5, and MT1_1_4) using both quantitative, real-time PCR (qRT-PCR) and chromatin fiber FISH. Genomic DNA was isolated using phenol/chloroform extraction. qRT-PCR was done using a Power SYBR green PCR Master mix (Applied Biosystems) and the iCycler machine (Bio-Rad Laboratories). Copy number was calculated using the absolute quantitation method (Ginzinger, 2002) with known concentrations of purified BAC DNA used to generate a standard curve. (Table S2 lists primers used). Stretched chromatin fibers were prepared as described elsewhere (Henry and Heng, 2002) and FISH was performed as described above.

Antibody staining

Cells were permeabilized in 0.1% Triton X-100/PBS* (CMF-PBS, 0.1 mM EDTA, and 5 mM $MgCl_2$) for 30 s before fixation in 1.6% formaldehyde/PBS* for 15 min at RT, blocked in 5% normal goat serum (Sigma-Aldrich)/PBS* for 1 h at RT followed by primary antibody incubation (mouse anti-ASF/SF2; Invitrogen), 1:200, or anti-SC35 (Sigma-Aldrich), 1:200, at 4°C overnight, three washes for 5 min, and secondary antibody (goat anti–mouse Texas red; The Jackson Laboratory), 1:1,000, for 4 h at RT, all in 0.1% Triton X-100/PBS*.

RNA extraction and RT-PCR

Total RNA was isolated using the RNeasy mini kit (QIAGEN) and on-column RNase-free DNase set (QIAGEN) according to the manufacturer's instructions. First-strand cDNA synthesis (ImProm-II kit; Promega) was performed using an oligo(dT) primer (Sigma-Aldrich). The comparative $2^{-\Delta\Delta Ct}$ method (Wong and Medrano, 2005) was used to measure relative expression levels. Table S2 lists primers used.

Transcription inhibition

Transcription was inhibited by incubating cells in 100 µg/ml α-amanitin (Sigma-Aldrich) for 3.5 h or 50 µg/ml DRB (Sigma-Aldrich) for 4.5 h in complete medium at 37°C before heat shock treatment for 30 min in the Hsp70_5 cell line. For the MT cell line, α-amanitin was added 2 h and DRB 3 h before the beginning of a 2-h zinc induction. Subsequently, cells were fixed in 1.6% formaldehyde/PBS for 30 min at RT, followed by three washes in PBS; the fixation procedure is the same as that without drug treatment (Fig. 2 A). In vivo labeling of RNA synthesis for confirmation of transcription inhibition used BrUTP incorporation as described elsewhere (Memedula and Belmont, 2003).

Microscopy and live observation

All samples after fixation were stained in 0.2 µg/ml DAPI and mounted in Prolong Antifade (Invitrogen). 3D optical section datasets of fixed cells were collected using a 60x objective (NA 1.4) on an inverted light microscope (IMT-2; Olympus) and deconvolved using an iterative algorithm as described previously (Tumbar et al., 1999). Live-cells maintained at 37°C in a closed chamber system (FCS2; Bioptechs) were imaged with a 63x objective (NA 1.40) using a Zeiss Axiovert 100M microscope equipped with a Roper CoolSNAP HQ slow-scan CCD camera (Roper Scientific).

Contour measurements were made from single optical sections from cells in which all GFP spots were visible and all spots in focus within a range of no more than two optical sections (0.2 µm depth). In fact, this applied to nearly all cells in the population, suggesting a nonrandom, polarized orientation of chromatin within the nuclei. In nearly all cases, at most one GFP spot was not in focus within the image, with the out of focus spot usually at one end or the other of the contour path. This allowed us to quickly make measurements from hundreds of cells per data point, while obtaining accurate estimates of contour lengths.

EM immunogold labeling used a new procedure (Kireev et al., 2008) in which primary mouse monoclonal IgG1κ anti-GFP or anti-Lac repressor antibodies or Fab′ fragments labeled covalently with Mono-Sulfo-NHS-Nanogold

(Nanoprobes) were microinjected into cells (Fab') or cell nuclei (IgG) together with 1.5 µg/µl Texas red–conjugated dextran (70 kD; Sigma-Aldrich). After microinjection cells were incubated at 37°C for 1 h before a brief detergent permeabilization in 0.1% Triton X-100, then fixed and processed for EM as described elsewhere (Kireev et al., 2008). TEM used a Phillips CM200 microscope using 120 kv for thin sections and 200 kv for thick sections, with images acquired using a TVIPS 2Kx2K Peltier-cooled CCD camera and software (Tietz Video and Image Processing Systems GmbH).

Online supplemental material

Figure S1: mitotic spreads and chromatin fiber FISH for three BAC transgene cell lines. Figure S2: statistics of transgene conformation before and after transgene activation. Figure S3: time course of Hsp70 BAC decondensation after heat shock. Video 1: movement of Hsp70 BAC transgenes during heat shock. Video 2: Speckle and Hsp70 transgene dynamics during heat shock. Video 3: Speckle dynamics during heat shock—nucleation of a new speckle. Video 4: Rapid, local chromatin movements are associated with conformational changes in the DHFR transgene array. Table S1: primers used for qPCR estimation of BAC copy number. Table S2: primers used for qRT-PCR determination of transgene expression levels. Table S3: primers used for DHFR gene probes (Fig. 4, D and E). Online supplemental material is available at http://www.jcb.org/cgi/content/full/jcb.200809196/DC1.

The content is solely the responsibility of the authors and does not necessarily represent the official views of the National Institute of General Medical Sciences or the National Institutes of Health. DHFR BACs were a gift from the laboratory of Edith Heard. pRSETB was a gift from the laboratory of Roger Tsien.

This work was supported by grant nos. GM58460 and GM42516 from the National Institute of General Medical Sciences awarded to A.S. Belmont.

Submitted: 29 September 2008
Accepted: 10 March 2009

References

Albrecht, A.L., R.K. Singh, S. Somji, M.A. Sens, D.A. Sens, and S.H. Garrett. 2008. Basal and metal-induced expression of metallothionein isoform 1 and 2 genes in the RWPE-1 human prostate epithelial cell line. *J. Appl. Toxicol.* 28:283–293.

Andersson, K., R. Mahr, B. Bjorkroth, and B. Daneholt. 1982. Rapid reformation of the thick chromosome fiber upon completion of RNA synthesis at the Balbiani ring genes in Chironomus tentans. *Chromosoma.* 87:33–48.

Beatty, B.G., and S.W. Scherer. 2002. Human chromosome mapping of single copy genes. *In* FISH: A practical approach. B. Beatty, S. Mai, and J. Squire, editors. Oxford University Press, Oxford. 29-53.

Belmont, A.S., and K. Bruce. 1994. Visualization of G1 chromosomes: a folded, twisted, supercoiled chromonema model of interphase chromatid structure. *J. Cell Biol.* 127:287–302.

Bjorkroth, B., C. Ericsson, M.M. Lamb, and B. Daneholt. 1988. Structure of the chromatin axis during transcription. *Chromosoma.* 96:333–340.

Bulger, M., D. Schubeler, M.A. Bender, J. Hamilton, C.M. Farrell, R.C. Hardison, and M. Groudine. 2003. A complex chromatin landscape revealed by patterns of nuclease sensitivity and histone modification within the mouse beta-globin locus. *Mol. Cell. Biol.* 23:5234–5244.

Callan, H.G. 1982. Lampbrush chromosomes. *Proc. R. Soc. Lond. B. Biol. Sci.* 214:417–448.

Carpenter, A.E., and A.S. Belmont. 2004. Direct visualization of transcription factor-induced chromatin remodeling and cofactor recruitment in vivo. *Methods Enzymol.* 375:366–381.

Chang, Y.C., S. Illenye, and N.H. Heintz. 2001. Cooperation of E2F-p130 and Sp1-pRb complexes in repression of the Chinese hamster dhfr gene. *Mol. Cell. Biol.* 21:1121–1131.

Chaumeil, J., I. Okamoto, and E. Heard. 2004. X-chromosome inactivation in mouse embryonic stem cells: analysis of histone modifications and transcriptional activity using immunofluorescence and FISH. *Methods Enzymol.* 376:405–419.

Chuang, C.H., A.E. Carpenter, B. Fuchsova, T. Johnson, P. de Lanerolle, and A.S. Belmont. 2006. Long-range directional movement of an interphase chromosome site. *Curr. Biol.* 16:825–831.

Chubb, J.R., S. Boyle, P. Perry, and W.A. Bickmore. 2002. Chromatin motion is constrained by association with nuclear compartments in human cells. *Curr. Biol.* 12:439–445.

Cmarko, D., P.J. Verschure, T.E. Martin, M.E. Dahmus, S. Krause, X.D. Fu, R. van Driel, and S. Fakan. 1999. Ultrastructural analysis of transcription and splicing in the cell nucleus after bromo-UTP microinjection. *Mol. Biol. Cell.* 10:211–223.

Dietzel, S., K. Zolghadr, C. Hepperger, and A.S. Belmont. 2004. Differential large-scale chromatin compaction and intranuclear positioning of transcribed versus non-transcribed transgene arrays containing beta-globin regulatory sequences. *J. Cell Sci.* 117:4603–4614.

Dubois, M.F., V.T. Nguyen, S. Bellier, and O. Bensaude. 1994. Inhibitors of transcription such as 5,6-dichloro-1-beta-D-ribofuranosylbenzimidazole and isoquinoline sulfonamide derivatives (H-8 and H-7) promote dephosphorylation of the carboxyl-terminal domain of RNA polymerase II largest subunit. *J. Biol. Chem.* 269:13331–13336.

Dundr, M., J.K. Ospina, M.H. Sung, S. John, M. Upender, T. Ried, G.L. Hager, and A.G. Matera. 2007. Actin-dependent intranuclear repositioning of an active gene locus in vivo. *J. Cell Biol.* 179:1095–1103.

Elgin, S.C.R. 1990. Chromatin structure and gene activity. *Curr. Opin. Cell Biol.* 2:437–445.

Ericsson, C., H. Mehlin, B. Bjorkroth, M.M. Lamb, and B. Daneholt. 1989. The ultrastructure of upstream and downstream regions of an active Balbiani Ring gene. *Cell.* 56:631–639.

Farnham, P.J., and R.T. Schimke. 1986. Murine dihydrofolate reductase transcripts through the cell cycle. *Mol. Cell. Biol.* 6:365–371.

Feder, J.N., Y.G. Assaraf, L.C. Seamer, and R.T. Schimke. 1989. The pattern of dihydrofolate reductase expression through the cell cycle in rodent and human cultured cells. *J. Biol. Chem.* 264:20583–20590.

Fiore, M., R. Zanier, and F. Degrassi. 2002. Reversible G(1) arrest by dimethyl sulfoxide as a new method to synchronize Chinese hamster cells. *Mutagenesis.* 17:419–424.

Forrester, W.C., T. Takegawa, G. Papayannopoulou, G. Stamatoyannopoulos, and M. Groudine. 1986. A developmentally stable chromatin structure in the human beta-globin gene cluster. *Proc. Natl. Acad. Sci. USA.* 83:1359–1363.

Ginzinger, D.G. 2002. Gene quantification using real-time quantitative PCR: an emerging technology hits the mainstream. *Exp. Hematol.* 30:503–512.

Henry, H., and Q. Heng. 2002. High resolution FISH mapping using chromatin and DNA fibers. *In* FISH: A Practical Approach. Oxford University Press, Oxford. 77–91.

Heun, P., T. Laroche, K. Shimada, P. Furrer, and S.M. Gasser. 2001. Chromosome dynamics in the yeast interphase nucleus. *Science.* 294:2181–2186.

Hidalgo, J., and J. Carrasco. 1998. Regulation of the synthesis of brain metallothioneins. *Neurotoxicology.* 19:661–666.

Iborra, F.J., A. Pombo, D.A. Jackson, and P.R. Cook. 1996. Active RNA polymerases are localized within discrete transcription "factories' in human nuclei. *J. Cell Sci.* 109(Pt 6):1427–1436.

Igo-Kemenes, T., W. Horz, and H.G. Zachau. 1982. Chromatin. *Annu. Rev. Biochem.* 51:89–121.

Iwanaga, R., H. Komori, and K. Ohtani. 2004. Differential regulation of expression of the mammalian DNA repair genes by growth stimulation. *Oncogene.* 23:8581–8590.

Jackson, D.A., A.N.A. Pombo, and F. Iborra. 2000. The balance sheet for transcription: an analysis of nuclear RNA metabolism in mammalian cells. *FASEB J.* 14:242–254.

Johnson, C., D. Primorac, M. McKinstry, J. McNeil, D. Rowe, and J.B. Lawrence. 2000. Tracking COL1A1 RNA in osteogenesis imperfecta. splice-defective transcripts initiate transport from the gene but are retained within the SC35 domain. *J. Cell Biol.* 150:417–432.

Jolly, C., C. Vourc'h, M. Robert-Nicoud, and R.I. Morimoto. 1999. Intron-independent association of splicing factors with active genes. *J. Cell Biol.* 145:1133–1143.

Kireev, I., M. Lakonishok, W. Liu, V.N. Joshi, R. Powell, and A.S. Belmont. 2008. In vivo immunogold labeling confirms large-scale chromatin folding motifs. *Nat. Methods.* 5:311–313.

Kireeva, N., M. Lakonishok, I. Kireev, T. Hirano, and A.S. Belmont. 2004. Visualization of early chromosome condensation: a hierarchical folding, axial glue model of chromosome structure. *J. Cell Biol.* 166:775–785.

Lawrence, J.B., R.H. Singer, and J.A. McNeil. 1990. Interphase and metaphase resolution of different distances within the human dystrophin gene. *Science.* 249:928–932.

Levi, V., Q. Ruan, M. Plutz, A.S. Belmont, and E. Gratton. 2005. Chromatin Dynamics in Interphase Cells Revealed by Tracking in a Two-Photon Excitation Microscope. *Biophys. J.* 89:4275–4285.

Litt, M.D., M. Simpson, M. Gasner, C.D. Allis, and G. Felsenfeld. 2001. Correlation between histone lysine methlation and developmental changes at the chicken beta-globin locus. *Science.* 293:2453–2455.

Ljungman, M., and P.C. Hanawalt. 1995. Presence of negative torsional tension in the promoter region of the transcriptionally poised dihydrofolate reductase gene in vivo. *Nucleic Acids Res.* 23:1782–1789.

Mahy, N.L., P.E. Perry, and W.A. Bickmore. 2002. Gene density and transcription influence the localization of chromatin outside of chromosome territories detectable by FISH. *J. Cell Biol.* 159:753–763.

Marshall, W.F., A. Straight, J.F. Marko, J. Swedlow, A. Dernburg, A. Belmont, A.W. Murray, D.A. Agard, and J.W. Sedat. 1997. Interphase chromosomes undergo constrained diffusional motion in living cells. *Curr. Biol.* 7:930–939.

Memedula, S., and A.S. Belmont. 2003. Sequential recruitment of HAT and SWI/SNF components to condensed chromatin by VP16. *Curr. Biol.* 13:241–246.

Misteli, T., J.F. Caceres, and D. Spector. 1997. The dynamics of a pre-mRNA splicing factor in living cells. *Nature.* 387:523–527.

Muller, W.G., D. Walker, G.L. Hager, and J.G. McNally. 2001. Large-scale chromatin decondensation and recondensation regulated by transcription from a natural promoter. *J. Cell Biol.* 154:33–48.

Muller, W.G., D. Rieder, G. Kreth, C. Cremer, Z. Trajanoski, and J.G. McNally. 2004. Generic features of tertiary chromatin structure as detected in natural chromosomes. *Mol. Cell. Biol.* 24:9359–9370.

Munkel, C., R. Eils, S. Dietzel, D. Zink, C. Mehring, G. Wedemann, T. Cremer, and J. Langowski. 1999. Compartmentalization of interphase chromosomes observed in simulation and experiment. *J. Mol. Biol.* 285:1053–1065.

Nguyen, V.T., F. Giannoni, M.F. Dubois, S.J. Seo, M. Vigneron, C. Kedinger, and O. Bensaude. 1996. In vivo degradation of RNA polymerase II largest subunit triggered by alpha-amanitin. *Nucleic Acids Res.* 24:2924–2929.

Olins, A.L., D.E. Olins, H.A. Levy, R.C. Durfee, S.M. Margle, and E.P. Tinnel. 1986. DNA compaction during intense transcription measured by electron microscope tomography. *Eur. J. Cell Biol.* 40:105–110.

Osborne, C.S., L. Chakalova, K.E. Brown, D. Carter, A. Horton, E. Debrand, B. Goyenechea, J.A. Mitchell, S. Lopes, W. Reik, and P. Fraser. 2004. Active genes dynamically colocalize to shared sites of ongoing transcription. *Nat. Genet.* 36:1065–1071.

Pecinka, A., N. Kato, A. Meister, A.V. Probst, I. Schubert, and E. Lam. 2005. Tandem repetitive transgenes and fluorescent chromatin tags alter local interphase chromosome arrangement in Arabidopsis thaliana. *J. Cell Sci.* 118:3751–3758.

Price, D.H. 2008. Poised Polymerases: On Your Mark...Get Set...Go! *Mol. Cell.* 30:7–10.

Ragoczy, T., A. Telling, T. Sawado, M. Groudine, and S.T. Kosak. 2003. A genetic analysis of chromosome territory looping: diverse roles for distal regulatory elements. *Chromosome Res.* 11:513–525.

Robinett, C.C., A. Straight, G. Li, C. Willhelm, G. Sudlow, A. Murray, and A.S. Belmont. 1996. In vivo localization of DNA sequences and visualization of large-scale chromatin organization using lac operator/repressor recognition. *J. Cell Biol.* 135:1685–1700.

Schilling, L.J., and P.J. Farnham. 1995. The bidirectionally transcribed dihydrofolate reductase and rep-3a promoters are growth regulated by distinct mechanisms. *Cell Growth Differ.* 6:541–548.

Shopland, L.S., C.V. Johnson, M. Byron, J. McNeil, and J.B. Lawrence. 2003. Clustering of multiple specific genes and gene-rich R-bands around SC-35 domains: evidence for local euchromatic neighborhoods. *J. Cell Biol.* 162:981–990.

Singh, R.K., A.L. Albrecht, S. Somji, M.A. Sens, D.A. Sens, and S.H. Garrett. 2008. Alterations in metal toxicity and metal-induced metallothionein gene expression elicited by growth medium calcium concentration. *Cell Biol. Toxicol.* 24:273–281.

Smith, K.P., M. Byron, C. Johnson, Y. Xing, and J.B. Lawrence. 2007. Defining early steps in mRNA transport: mutant mRNA in myotonic dystrophy type I is blocked at entry into SC-35 domains. *J. Cell Biol.* 178:951–964.

Solevei, I., M. Walter, M. Cremer, F. Habermann, L. Schermelleh, and T. Cremer. 2002. FISH on three-dimensionally preserved nuclei. *In* FISH: A Practical Approach. B. Beatty, S. Mai, and J. Squire, editors. Oxford University Press, Oxford. 119–154.

Spring, H., and W.W. Franke. 1981. Transcriptionally active chromatin in loops of lampbrush chromosomes at physiological salt concentrations as revealed by electron microscopy of sections. *Eur. J. Cell Biol.* 24:298–308.

Tumbar, T., G. Sudlow, and A.S. Belmont. 1999. Large-scale chromatin unfolding and remodeling induced by VP16 acidic activation domain. *J. Cell Biol.* 145:1341–1354.

Urlaub, G., P.G. Mitchell, E. Kas, L.A. Chasin, V.L. Funanage, T.T. Myoda, and J. Hamlin. 1986. Effect of gamma rays at the dihydrofolate reductase locus: deletions and inversions. *Somat. Cell Mol. Genet.* 12:555–566.

Vazquez, J., A.S. Belmont, and J.W. Sedat. 2001. Multiple regimes of constrained chromosome motion are regulated in the interphase Drosophila nucleus. *Curr. Biol.* 11:1227–1239.

Volpi, E.V., E. Chevret, T. Jones, R. Vatcheva, J. Williamson, S. Beck, R.D. Campbell, M. Goldsworthy, S.H. Powis, J. Ragoussis, et al. 2000. Large-scale chromatin organization of the major histocompatibility complex and other regions of human chromosome 6 and its response to interferon in interphase nuclei. *J. Cell Sci.* 113:1565–1576.

Wong, M.L., and J.F. Medrano. 2005. Real-time PCR for mRNA quantitation. *Biotechniques.* 39:75–85.

Yokota, H., G. van den Engh, J.E. Hearst, R.K. Sachs, and B.J. Trask. 1995. Evidence for the organization of chromatin in megabase pair-sized loops arranged along a random walk path in the human G0/G1 interphase nucleus. *J. Cell Biol.* 130:1239–1249.